Comparing chloride ingress from seawater and NaCl solution in Portland cement mortar

De Weerdt, K.[1], Lothenbach, B. [1,2], Geiker, M. R. [1]

[1]Department of Structural Engineering, NTNU, Norway

[2]EMPA, Dübendorf, Switzerland

Abstract

This study investigates whether chloride ingress testing using NaCl solution is conservative when assessing the performance of concrete in marine conditions. Seawater contains besides sodium and chlorine additional elements such as sulfur and magnesium, which can change the phase assemblage in the concrete and thereby affect chloride ingress. Mortars samples prepared with Portland cement were exposed to seawater or NaCl solution with a similar chloride concentration. After 180 days of exposure to seawater, only the outer 1 mm was enriched in sulfur and magnesium, which had only a limited impact on the chloride ingress. Leaching, observed in the outer 10-20 mm both for NaCl and for seawater exposure had a much stronger influence on the chloride ingress. Hence, chloride ingress in marine exposed concrete can be assessed using NaCl solutions. To mirror the leaching in field exposure, the volume of exposure solution needs to be high.

Keywords: B. EDX; B. Thermal Analysis; C. Durability; D. Chloride; thermodynamic modelling

1 Introduction

Reinforced concrete is an important construction material for marine exposed structures such as bridges, docks, harbours, off shore and platforms due to its ability to withstand the harsh marine environment. However, the service life of reinforced concrete structures can be limited by several deterioration mechanisms. In marine environment, one of the major deterioration mechanisms is chloride induced corrosion of the reinforcement steel. When chlorides reach the reinforcement and accumulate to critical concentrations they can initiate corrosion. Hence, to ensure sufficient service life, such structures need to be designed and constructed with concrete compositions with high chloride ingress resistance, as well as an appropriate concrete cover depth in order to protect the reinforcement during the designed service life.

Laboratory testing of concrete compositions for marine applications is generally performed with NaCl solutions to mimic the marine conditions. Commonly used diffusion tests either prescribe exposure to 3% NaCl solution (approx. 30 g/l), which yields a similar chloride concentration as in the Atlantic,

(ASTM C1543 [1], EN 13396 [2], CEN/TS 12390-11 [3]) or about 5.5 times higher concentration (165 g/l NaCl solution), (ASTM C1556 [4] and NT BUILD 443 [5]).

However, seawater contains, in addition to sodium and chloride, other ions, for example magnesium, sulfate, and carbonates, which potentially can influence the chloride ingress [6]. The effect of seawater on the phase assemblage of concrete is complex. The differences in the mobility of the ions and in the solubility of the reaction products results in elemental zonation in the concrete near the surface [7-11].

In this study, we investigated whether the presence of ions other than sodium and chloride in seawater will affect the chloride ingress. The chloride ingress by bulk diffusion in Portland cement mortars exposed to seawater is compared with mortars exposed to NaCl solution with a similar chloride concentration. Saturated samples were exposed to seawater and NaCl solution 7 days after casting. Elemental profiles were determined after 21, 90 and 180 days of exposure at 20^{o}C.

2 Experimental

2.1 Materials

Mortars with ordinary Portland cement (PC) type CEM I 42.5 R according to EN197-1 [12] with 6% silica fume (SF) were investigated. The mix composition of the mortars is given in Table 1**Error! Reference source not found.**.

The chemical composition of the different materials is given in Table 2. Table 3 gives the mineral composition of the Portland cement determined by XRD-Rietveld. About 99.2% of the silica fume is X-ray amorphous. The PC mortar was proportioned with a water-to-binder mass ratio of 0.40 and the sand-to-binder mass ratio of 2.5:1. A polycarboxylate based superplastisizer (SP) was included to obtain good compactability, while air demper was added to reduce the amount of entrapped air. The amount of mixing water was corrected for the water present in the admixtures (SP and demper). Standard sand according to EN196 [13] was used for all the mixes.

For the exposure, two kinds of solutions were used: seawater and NaCl solution. The seawater was taken from the Trondheim fjord, Norway. The composition of the seawater determined by inductive coupled plasma mass spectrometry (ICP-MS) is given in Table 4. The NaCl solution was prepared using technical grade NaCl and distilled water to have the same chloride concentration as the seawater. The chloride concentration of the NaCl concentration was checked by $AgNO_3$ titration (see Table 4).

2.2 Sample preparation

The mix compositions are given in Table 1**Error! Reference source not found.**. The mortars were mixed with a Hobart mixer (10 L mixing bowl). The volume of the mortar batches was 2.7 L. The mixing procedure was the following: The cement and sand are first dry mixed for ½ minute at speed I. During the following ½ minute the water including the admixtures was added to the bowl while mixing at speed I. Then the mortar was mixed for an additional minute at speed I, and after a break of three minutes the mortar was mixed for one more minute at speed II.

After mixing, the samples were filled into 125 mL cylindrical sealed HDPE bottles and stored in a 20°C acclimatized room. After 1 day, a small amount of water was added in the bottom and at the top of the bottle, in order to counteract self-desiccation (see Figure 1). Most of the samples were prepared for exposure as described below, however some samples were cured sealed for longer time at 20°C and used as non-exposed references.

2.3 Exposure to NaCl and seawater

For the exposed samples, the plastic bottles were removed after 3 days of curing. After demoulding, the top 10 mm of each sample was sawn off and the samples were placed on grids and dried in a desiccator over silica gel for 2 hours. The dried samples were coated with two layers of epoxy and put to dry in air for 24 hours on small studs after applying each layer of coating. During the epoxy coating the samples dried. Therefore the 5 days old coated samples were placed in distilled water for 2 days in order to saturate them prior to exposing them to the NaCl solution and seawater. This was done in order to limit capillary suction of the exposure solutions and isolate diffusion as a sole ingress mechanism.

The samples were stored in sealed boxes resting on a grid, 2-3 mm submerged in the exposure solutions, with the epoxy-free surface facing down wards as shown in Figure 2. The sealed boxes contained approx. 500 ml exposure solution for 12 samples (exposure surface of approx. 236 cm^2). The exposure solution was exchanged weekly.

The samples were investigated after 21, 90 and 180 days of exposure. For each time, three samples were investigated per exposure solution. One of the three samples was split. One half was sprayed with 0.1 M $AgNO_3$ to have an indication of the Cl-ingress depth. This half was also used for the preparation of a thin section (see Figure 2). The other half and the two remaining samples were profile ground. Prior to profile grinding, the epoxy on the cylindrical surface was removed by grinding. The profile grinding was performed with the following intervals 0-1, 1-3, 3-5, 5-7, 7-9, 9-13, 13-17, 17-23 mm. The ground samples were stored in plastic grip-bags which were placed in a desiccator until analysis. Chloride analysis was performed on all three sample i.e. the two full and one half samples, whereas thermogravimetric analysis (TGA) and induced coupled plasma mass spectrometry (ICP-MS) was only performed on one of the samples.

2.4 Reference samples

Two different sets of non-exposed reference samples were used. One reference sample was taken after 180 days of sealed curing at 20°C. The sample was crushed and ground, and analysed with the same methods as the profiles ground sections of the exposed samples (see section 2.5). After 3 years of sealed curing at 20°C, the other non-exposed reference mortar sample was used for pore solution extraction using a steel die method described in [14]. The pore solution composition was analysed by ICP-MS.

2.5 Analysis of mortars

Approx. 5 g of each profile ground section was used to determine the acid soluble chloride content which we refer to as the total chloride content. The powder was weighed prior and after drying at 105°C overnight in order to determine the free moisture content. The dried powder was dissolved in 50 mL 80°C (1:10) HNO_3, and filtrated after 1 hour. The chloride content in the resulting filtrate was determined by potentiometric titration with a Titrando 905 titrator from Metrohm using 0.01 M $AgNO_3$ and expressed relative to the dry concrete mass (mass after drying at 105°C).

The filtrate obtained from the acid digested ground mortar powder produced for the chloride analysis was also used for determining the total content of potassium (K), sodium (Na), magnesium (Mg), and sulfur (S) using a ICP-MS Element 2 from Thermo Scientific. The concentrations of the various elements measured were recalculated relative to the dry concrete mass (weight after drying at 105°C).

The thermogravimetric analysis (TG) was performed with a Mettler Toledo TGA/SDTA851, on approximately 300 mg of the profile ground samples loaded in 900 µL alumina crucibles. The samples were heated up from 40 to 900°C at a rate of 10°C/min while the oven was purged with N_2 at 50 ml/min. The mass loss of the samples was monitored as a function of the temperature. The mass loss due to the release of water (H), decomposition of calcium hydroxide (CH), and release of CO_2 was measured in the respective temperature intervals 40-550°C, 450-550°C, and 550-850°C. The exact limits for the temperature intervals were determined based on the derivative thermogravimetric curves (DTG). All results were expressed relative to the mass of the concrete powder samples at 850°C. The amount of calcium hydroxide is calculated by multiplying the weight loss with 74/18 (molar mass $Ca(OH)_2$ / molar mass H_2O).

The polished thin sections were investigated with a Hitachi S-3400N scanning electron microscope (SEM) operated at an accelerating voltage of 15 kV combined with an Oxford 80 mm^2 X-MaxN SD energy dispersive spectrometer (EDS) with 125 eV spectral resolution. In this paper, elemental EDS maps of the surface near region of a selection of samples are presented.

2.6 Thermodynamic modelling

Thermodynamic calculations were carried out using the Gibbs free energy minimization software GEMS3 [15, 16], which is a geochemical modelling code that computes equilibrium phase assemblages and speciation in complex chemical systems. The general thermodynamic database [17, 18] was expanded with the Cemdata18 database [19], which contains solubility products of solids

relevant for cementitious systems. The data-set includes thermodynamic data for common cement minerals such as ettringite (AFt) and alumina-ferric monophases (AFm), hydrotalcite, hydrogarnet and C–S–H phases. The C–S–H phases were modelled using the CSHQ model developed by Kulik [20], which is based on a continuous solid solution between four C-S-H end-members with different Ca/Si ratios resulting in C-S-H phases with Ca/Si ratios between 0.6 to 1.6. Data for magnesium silicate hydrates (M-S-H) were taken from Nied et al. [21], who also used a solid solution model, and data for Na- and Ca containing zeolites from Lothenbach et al. [22]. The formation of magnesite, dolomite, quartz, aluminium containing siliceous hydrogarnet and thaumasite was suppressed in the modelling due to their slow formation kinetic at ambient temperature.

To simulate the effects of NaCl or seawater on the hydrate assemblage, the hydrated cement was virtually titrated with volumes of NaCl solution or seawater as described in detail in [23, 24]. The quantity of NaCl solution in the calculations was varied from 0 to 200'000 ml solution per 100 g anhydrous cement and the results are presented in g per 100 g anhydrous cements as a function of the volume of the added solution. This approach allows prediction of the progressive changes in phase assemblage upon ingress of chloride and other ions, assuming that the surface of the mortar is in contact with a very high amount of NaCl or seawater solution and that the center of the mortars comes into contact with very low amounts of solution only. The concentrations used in the modelling were those compiled in Table 4.

158 **3 Results**

159 **3.1 Chloride profiles**

160 Figure 3 shows the chloride profiles for mortar exposed to seawater (dashed lines) and to NaCl
161 solution (solid lines) for 21, 90 and 180 days.

162 For all exposure times, seawater exposure (dashed lines) seems to lead to a higher chloride content
163 compared to exposure to NaCl solution (solid line) at the same depth from the exposed surface.

164 Over time the chloride profiles start to show a reduction in the chloride content at the surface (0-1
165 mm section) compared to the chloride content deeper in (e.g. section 1-3 mm).

166 Chloride content was determined using titration and also by ICP-MS. The concentrations obtained by
167 the two techniques are in relatively good agreement as can be seen from Figure 4. It should be noted
168 that three parallel samples were analysed by titration whereas only one of these samples was
169 analysed by ICP-MS.

170

171 **3.2 Total elemental profiles determined by ICP-MS**

172 The sections analysed by chloride titration were also analysed for different elements by ICP-MS.
173 Figure 5 shows the elemental concentration of sodium (Na), potassium (K), magnesium (Mg) and
174 sulfur (S) determined by ICP-MS for the mortar samples after 21, 90 and 180 days of exposure to
175 seawater (dashed lines) and NaCl solution (solid lines). Only four sections were analysed per sample
176 namely 0-1 mm, 1-3 mm, 3-5 mm and 5-7 mm. In addition, one non-exposed reference sample was
177 analysed to determine the background level of the elements. In the graphs the background is
178 depicted at a depth of 15 mm. The sand will merely have diluting function on the elemental profiles
179 depicted in Figure 5, as the elemental changes will take place in the cement paste and a relatively
180 pure siliceous sand is used (Table 2). In addition, it should be noted that the exposed surface is a cut
181 surface. Therefore there should be no systematic differences in the paste content of the different
182 investigated sections which could cause gradients in the elemental composition.

183 In order to identify concentration gradients between the exposure solutions and the pore solution of
184 the mortars, the pore solution was obtained from non-exposed samples sealed cured for 3 years (see
185 Table 5).

186 Both exposure solutions, seawater and NaCl solution, have a more than 3-times higher sodium
187 concentration (Table 4) than the pore solution of the mortars (Table 5), therefore sodium was
188 expected to diffuse into the samples. However, the sodium profiles show enrichment in sodium only
189 for the samples exposed to NaCl solution, and just in the outer most section (0-1 mm). In the sections

190 further from the surface the sodium content was at the background level. Hence, no clear diffusion
191 profiles can be observed for sodium within the scale of the analysed sections (1 or 2 mm). The
192 sodium content in the outermost layer seems to increase with increasing exposure time, although
193 the changes were limited between 90 and 180 days exposure. In the case of exposure to seawater,
194 on the other hand, there is no enrichment in sodium in the outermost section for all investigated
195 times, contrary there is even slight indication of sodium leaching towards the surface.

196 The NaCl solution does not contain potassium, and the seawater only very low concentrations (Table
197 4) compared to the potential pore solution of the mortar (Table 5). Hence, potassium profiles do
198 show clear leaching profiles for all samples. The background level of potassium was maintained in the
199 section 5-7 mm up to 21 and 90 days of exposure. Prolonged exposure, 180 days, led to further
200 leaching as potassium level at the depth of 5-7 mm dropped below the background level.

201 Magnesium is present in the seawater, but not in the NaCl solution. Hence, ingress of magnesium in
202 the mortar samples exposed to seawater is expected. However, magnesium is hardly mobile in the
203 high pH environment of the mortar, and it is therefore unlikely to diffuse deep into the samples. In
204 fact, the outermost sections (0-1 mm) of all samples exposed to seawater show an enrichment in
205 magnesium, whereas the magnesium level in the NaCl exposed samples remains unchanged. There is
206 no clear increasing trend in the magnesium content in the outermost section of the seawater
207 exposed samples with exposure time larger than 90 days.

208 The NaCl solution does also not contain sulfur, whereas the seawater contains slightly more (Table 4)
209 compared to the pore solution of the unexposed mortar (Table 5). The sulfur profiles show that the
210 sulfur content only increased in the outermost section (0-1 mm) for the samples exposed to
211 seawater. Exposure to NaCl solution did result in an apparent minor reduction in the sulfur content in
212 the outer approximately 5 mm. For the seawater exposed samples, similar observations were made
213 as for magnesium: also the sulfur content did not increase further with time after 21 days of
214 exposure.

215

216 **3.3 Phase assemblage**

217 The TGA analysis of the inner part of mortars hydrated for 90 days (13-17 mm in Figure 6) showed
218 that the hydrated mortars contained C-S-H, portlandite (approx. 4 wt.%), some ettringite, calcium
219 carbonate as well as monocarbonate. In the sections 1-3 and 3-5 mm the main phase changes, for
220 both NaCl and seawater exposure, were a reduction in the portlandite content and the formation of
221 Friedel's salt. However, in the outer most section, 0-1 mm, the phase changes were different for the
222 different exposure solutions. For both exposures we observed a reduction in portlandite, and the

223 presence of Friedel's salt and carbonates, but in the case of seawater in addition an enrichment in
224 ettringite, and brucite.

225 Figure 7 shows the portlandite and carbonate profiles determined by TGA. The carbonate profiles
226 showed an increase in the carbonate content in the outermost section (0-1 mm) for all investigated
227 samples. In the case of NaCl exposure the enrichment in carbonates is most likely due to carbonation
228 during sample preparation i.e. during drying when applying the epoxy coating. The increase in
229 carbonates is more pronounced for seawater exposure probably due to the presence of dissolved
230 carbonate in the seawater (Table 4). This is also reflected in the increase of the amount of carbonates
231 with exposure time.

232 The amount of portlandite was reduced towards the exposed surface for all samples. The decrease in
233 the outermost section will be partially due to the carbonation of this section. The gradual decrease in
234 portlandite in the deeper lying uncarbonated sections is caused by leaching. The leaching was
235 independent of whether the samples were exposed to seawater or NaCl solution. In addition the
236 leaching progressed with increasing exposure time.

237

238 **3.4 SEM-EDS elemental maps**

239 Figure 8 and Figure 9 show a BSE image and the elemental maps for the samples exposed to
240 respectively seawater and NaCl solution for 90 days. These maps illustrate the elemental changes
241 taking place in the outer mm of the mortar of the seawater and NaCl exposed samples. They are
242 representative for other samples investigated at different exposure times. In both sets of maps it can
243 be clearly seen that the siliceous sand was used to prepare the mortars; calcium represents the
244 cement paste in the mortar.

245 The seawater exposed sample does not show an increased porosity at the exposed surface.
246 Elemental zonation is observed: on the surface deposits of a magnesium rich phase, i.e. brucite, as
247 well as calcium carbonate crystals are observed. In the deposited layer a slight enrichment of sodium
248 was observed which was, however, not reflected in the profiles in Figure 5. Just below the surface
249 deposits, the paste showed a slight sulfur enrichment and further in a chlorine enrichment.

250 For the NaCl exposed sample, the outer surface has become more porous (darker in BSE). The outer
251 100 µm section are leached for calcium and sulfur and also the chloride level is low in this region. The
252 sodium content, on the other hand, is clearly increased in this zone, in agreement with the ICP-MS
253 analysis.

254

3.5 Modelling of phase changes

Thermodynamic modelling is used to calculate the effect of NaCl or seawater on the hydrates (Figure 10). The right hand side of the figures displays the paste composition in the unaffected core of the mortar; to the left the effect of more NaCl or seawater solution on the hydrates formed is calculated, which represents the gradual changes towards the surface of a exposed mortar. The vicinity of the exposed surface is simulated in the thermodynamic model by increasing the amount of exposure solution (up to 100 kg / 100 g cement).

For the non-exposed core of the sample, the predicted phase composition consists of C-S-H, portlandite, ettringite, monocarbonate, siliceous hydrogarnet and calcium carbonate. Upon exposure to NaCl solution, first Friedel's salt forms instead of monocarbonate. For higher levels of NaCl solution all phases decompose, leading to a gradual reduction of the total volume of solid phases. At very high NaCl levels alkali aluminium silicates are predicted to form, in this case represented by the zeolite natrolite.

In the case of seawater, we similarly predict the formation of Friedel's salt instead of monocarbonate for low levels of seawater. However, upon higher levels of seawater there is an increase in the total volume of phases even though portlandite decomposes. This is caused by the formation of phases such as ettringite, calcite and brucite due to the presence of sulfate, carbonate and magnesium in the seawater. For even higher levels of seawater, C-S-H and ettringite decompose and instead additional M-S-H, hydrotalcite, brucite and calcite are formed resulting in a reduction of the total volume of phases.

Figure 11 shows the predicted portlandite and carbonate profiles as a percentage of the dry mortar mass (including modelled bound water), and Figure 12 the elemental profiles for the same simulations (including 10 ml of the modelled exposure solution per 100 g cement in addition to the modelled bound water) to correspond to the experimental elemental profiles shown in Figure 3 and Figure 5.The predicted phase assemblage and profiles are compared to the experimental results in the discussion.

4 Discussion

4.1 Changes in the phase assemblage

The predicted phase composition of the non-exposed sample consists of C-S-H, portlandite, ettringite, monocarbonate, siliceous hydrogarnet (Si-Hg) and calcite (right hand side in Figure 10 at approx. 0 g NaCl or seawater). This corresponds to the phases observed using TGA (Figure 6 section 13-17 mm) except for the siliceous hydrogarnet which cannot easily be identified using TGA, as it shows a broad weight loss in the temperature region 300-400°C, where also hydrotalcite and C-S-H phases show a weight loss. The modelled portlandite content is lower (Figure 11) than the amount measured by TGA (Figure 7), which can be related to differences in the Ca/Si of the C-S-H in the model (Ca/Si = 1.6) and the actual Ca/Si.

The measured total content of sodium, potassium and sulfur determined in the non-exposed sample (Figure 5) agrees very well with the predicted content in Figure 12. The discrepancy between the predicted and measured magnesium content is due to the omission of the magnesium originating from the cement in the model.

Upon exposure to either seawater or NaCl solution, one can observe a reduction in portlandite and the formation of Friedel's salt using TGA (section 1-3 and 3-5 mm in Figure 6 and Figure 7). In the model this corresponds to the phase assemblage at an addition of seawater or NaCl solution in the range of 20 to 200 g in Figure 10 and Figure 11. However, at the exposed mortar surface, i.e. the outermost section 0-1 mm, the phase changes differ for the two exposure conditions. The phase changes experimentally observed in the outermost section correspond to the changes up to approximately 10 000 g of NaCl solution and 1000 g of seawater in Figure 10 and the corresponding elemental changes up to approximately the same limits in Figure 12.

Upon exposure to even higher levels of seawater, the model predicts a decrease in Friedel's salt in parallel to a decrease in portlandite, combined with an increase in ettringite, and finally for very high seawater additions, a decomposition of ettringite and C-S-H and the formation of gypsum, M-S-H, brucite, and calcite.. In agreement with the modelling, we observed for seawater exposure a sulfur enrichment by SEM-EDS (Figure 8) and ICP-MS (Figure 5) near the surface, which is due to the formation of ettringite as confirmed also by the TGA data (Figure 6). The precipitation of brucite and calcite on the exposed surface was confirmed both by SEM-EDS (Figure 8) and TGA (MH and carbonate in Figure 6 and Figure 7). Brucite formation was also reflected in the increase in the measured magnesium content in the outermost section (Figure 5 and Figure 12). The predicted (Figure 10) decomposition of ettringite and C-S-H, and the formation of M-S-H were not experimentally observed as it would occur at even higher levels of leaching than the one observed

315 within the applied exposure time. In other studies, M-S-H has been observed in concrete within 5
316 years of exposure to seawater [25]. The discrepancy between the modelled chlorine level (Figure 12)
317 and the maximum measured chlorine content (Figure 3) is attributed to the fact that the model only
318 accounts for chloride binding in Friedel's salt (Figure 10) and not for the potential chlorine in C-S-H.

319 In the case of NaCl solution exposure, portlandite, ettringite, Friedel's salt and C-S-H are predicted to
320 decompose together with the formation of natrolite or an amorphous precursor at the surface
321 (Figure 10). The SEM-EDS maps confirm the leaching of calcium-containing phases, e.g. C-S-H,
322 ettringite and Friedel's salts, in the outermost 100 µm (Figure 9). The extremely leached zone is
323 deprived of calcium, sulfur and chlorine, but contains still silicon, aluminium and sodium. This points
324 towards the formation of an alkali containing aluminium silicate phase (e.g. natrolite or an
325 amorphous zeolitic precursor) at the exposed surface. This also corresponds to the increase in both
326 the measured and predicted sodium content (Figure 5 and Figure 12) near the surface within the
327 NaCl exposed sample.

328 Leaching during both NaCl solution and seawater exposure is demonstrated by the reduction in
329 portlandite and potassium towards the exposed surface as predicted (Figure 11 and Figure 12) and
330 experimentally confirmed (Figure 7 and Figure 5). The leaching seems to be independent of whether
331 the samples are exposed to seawater or NaCl solution, and progresses with increasing exposure time.

332

333 **4.2 Diffusion of elements in mortar**

334 When comparing the pore solutions of the unexposed mortars in Table 5 with the exposure solutions
335 in Table 4, the largest differences can be found for the chlorine and the potassium concentrations.
336 The exposure solution has a chlorine concentration, which is approx. two orders of magnitude larger
337 than the concentration in the pore solution, while for the potassium the concentration in the
338 exposure solution is minimum one order of magnitude lower than in the pore solution of the
339 unexposed mortar. The differences in concentration of sulfur, magnesium and sodium are smaller.

340 Thus, the total potassium and chlorine exhibited clear diffusion profiles and the profiles changed with
341 time. Chlorine was ingressing (Figure 3) while potassium was leaching (Figure 5), independent
342 whether NaCl or seawater was the exposure solution.

343 The other elements, magnesium, sulfur, and sodium, were enriched in the outermost section (0-1
344 mm) (Figure 5). The applied grinding techniques do not have sufficient spatial resolution to allow
345 measurement of diffusion profiles for these elements. It becomes however evident that sulfur and
346 magnesium move much less in the mortar than chlorine and potassium. The precipitation of
347 magnesium as brucite occurs at pH values higher than 10 [26] and leads to very low magnesium

concentrations at high pH values. Therefore, the magnesium has very limited mobility in cementitious systems with high pH. In fact, the precipitation of magnesium hydroxide is observed on the surface of the cement and its content in the cement paste does not seem to increase significantly within the investigated exposure time. Sulfur progressed somewhat further, but also for sulfur the content and penetration depths did not increase within the exposure time, which however might rather be related to the limited lateral resolution due to the used grinding technique.

Sodium shows a particular behaviour, there is an increase in the content with time within the mortar near the surface, but only for the NaCl exposure. In the case of seawater exposure, which contains a comparable sodium concentration, there is no clear enrichment in sodium. The enrichment in the case of exposure to the NaCl solution would be consistent with the calculated formation of natrolite or a zeolitic precursor near the surface, which is only possible when the paste is strongly decalcified. In the case of seawater the decalcification of C-S-H at the exposed surface is less severe and therefore no natrolite formation is predicted and no sodium enrichment within the mortar is observed. In addition, the decalcification of C-S-H at the surface could also allow for additional sodium binding in the C-S-H, as low Ca/Si C-S-H is able to bind more alkali [27]. The good agreement between modelled behaviour and experimental observation also indicates that the elemental profiles we are measuring, reflect to a large extent the interaction between the different elements and the solids, and only to a limited extent the content of an element in the pore solution.

4.3 Do sulfur and magnesium enrichment stop chloride ingress?

From the chloride profiles (Figure 3) it can be seen that there was no increase in the resistance to chloride ingress of the mortars when exposed to seawater compared to NaCl solution. Even to the contrary, the total chlorine contents for the seawater exposed samples are higher than for the NaCl exposed samples at the same depth from the exposed surface although the seawater exposed samples had a clearly more intact microstructure at the surface. Hence, although sulfur and magnesium present in seawater are able to stabilise the microstructure at the surface they do not prevent or slow down chloride ingress.

Others [6] have observed enhanced chloride ingress upon exposure to combinations of magnesium sulfate and NaCl, but this might be due to the high sulfate concentrations used (350 mmol/l sulfur), which over time led to cracking due to sulfate attack opening up for chloride ingress. A recent survey of Norwegian and Danish marine exposed concretes showed that for the sulfur concentration present in seawater of 30 mmol/l, and low water-binder-ratios applied for marine concrete, generally just an enrichment in sulfur is observed near the surface, but no or only limited signs of damage [25,

28]. It is therefore important to use realistic sulfur and magnesium concentrations to assess their effect on chloride ingress.

Similarly, the microstructure stabilised by carbonate, sulfur and magnesium did not prevent or reduce leaching as demonstrated by the portlandite profiles determined by TGA. There was no significant difference between the samples exposed to seawater and NaCl solution using this technique.

4.4 Shape of the chloride profile

A beginning peaking behaviour of the chloride profiles is observed after 90 days for the seawater exposed samples and after 180 days for the NaCl exposed samples. For the samples exposed to seawater for 180 days, the chloride content in the outermost section (0-1 mm) is lower than the chloride content at 1-3 mm. In the case of seawater, one could attribute this to the ingress of sulfur which reduces the chloride binding capacity [29-31]. However, the peaking behaviour is also observed for the samples exposed to NaCl solution, which does not contain sulfur. Also carbonation can reduce the chloride binding capacity [30], however the peaking behaviour for NaCl exposure becomes more pronounced with time whereas the level of carbonation remains the same.

The fact that over time the chlorine content becomes slightly lower at the surface compared to the section deeper in is attributed to severe leaching in the outermost zone of the samples as seen in the elemental maps in Figure 8 and Figure 9. This leads to the decomposition of C-S-H and the loos of its ability to sorb chlorine.

The chloride profiles also exhibit an increase in the maximum chlorine content over time. Our hypothesis is that leaching leads to a reduction in the pH and partial decalcification of the C-S-H causing an increase in the calcium concentration in the pore solution, which on its turn leads to increased chloride binding. It has been recently shown that the availability of calcium plays a fundamental role in the ability of cement to bind chloride, and that a decrease in the availability of calcium lowers the amount of chlorine associated with C-S-H [32,33].

As leaching and the consequent decalcification of C-S-H influences the chloride ingress profile, it is important to allow leaching during testing. This can be done by keeping the volume of the exposure solution high enough and the composition constant to simulate field exposure, e.g. concrete column in the sea.

4.5 Impact of the findings for service life modelling

The presence of sulfate, magnesium and carbonate in the seawater in addition to sodium and chlorine did not have a major effect on the chloride ingress within the 180 days of exposure at 20°C. This supports the use of NaCl solution when testing the resistance to chloride ingress from marine exposed concrete.

The changes in the phase composition in the exposed concrete can give rise to variations in the value and location of the maximum chloride concentration and potentially also the diffusion coefficient over time, both for seawater and NaCl solution. We attribute the increase in the maximum chloride content and inwards movement of the maximum chlorine content in concrete to progressed decalcification of the C-S-H.

In service life models based on Fick's second law of diffusion, e.g. as used in [fib 2006], describing the chloride ingress profiles with two parameters, a surface concentration C_s and an apparent diffusion coefficient D_{app}, the impact of these time dependent changes are currently mathematically taken into account by an "ageing factor" applied on the apparent diffusion coefficient. However, also the surface concentration changes over time as the value and location of the maximum chloride content strongly affect the surface concentration.

It can be concluded that in order to understand and predict chloride ingress over time, multi-species ingress models taking into account changes in the phase assemblage over time are needed.

5 Conclusion

The aim of this study was to investigate how elements in seawater other than chlorine and sodium affect chloride ingress in cement-based materials over time. This was done by comparing chloride ingress in mortar from seawater with the ingress from a NaCl solution with the similar chlorine content at 20°C during 180 days. The samples were saturated prior to exposure in order to avoid capillary suction and to focus on diffusion as a sole ingress mechanism. We observed that:

- Phase changes due to the presence of sulfur and magnesium in seawater did not limit chloride ingress within the investigated time range.
- Peaking behaviour in the chloride profiles seems to be due to leaching causing decalcification of the C-S-H.
- Chlorine and potassium showed clear diffusion profiles up to 10-20 mm depth, whereas ingress of sodium, sulfur and magnesium was limited to the outer 1 mm at the surface.

Acknowledgements

The authors would like to acknowledge COIN, the COncrete INnovation center, for facilitating this research project. Denisa Orsakova, Department of Civil Engineering, Technical University of Brno, Czech Republic, is gratefully acknowledged for assisting in the experimental work. Syverin Lierhagen from NTNU is thanked for performing the ICP-MS analysis.

References

[1] ASTM C1543-10, Standard test method for determining the penetration of chloride ion into concrete by ponding, in, ASTM Internatinal, West Conshohocken, PA, 2010.

[2] EN 13396, Products and systems for protection and repair of concrete structures - Test methods - Measurement of chloride ion ingress, in, European committee of standardisation, Brussels, 2004.

[3] CEN/TS 12390-11, Testing hardened concrete - Part 11: Determination of chloride resistance of concrete, unidirectional diffusion, in, European committtee for standardisation, Brussels, 2010.

[4] ASTM C1556-11a, Standard test method for determining the apparent chloride diffusion coefficient of cementitious mixtures by bulk diffusion, in: A. International (Ed.), ASTM Internatinal, West Conshohocken, PA, 2011.

[5] NT BUILD 443, Concrete, Hardened: Accelerated chloride penetration, in: Nordtest (Ed.), Espoo, 1995.

[6] M. Maes, F. Mittermayr, N. De Belie, The influence of sodium and magnesium sulphate on the penetration of chlorides in mortar, Mater Struct, 50 (2017).

[7] R. Duval, H. Hornain, Chapter 9: La durabilité des bétons vis-à-vis des eaux agressives in: J. Baron, J.P. Ollivier (Eds.) Durabilité des bétons, Presses de l'École Nationale des Ponts et Chaussées, 1992, pp. 351-394.

[8] J. Marchand, E. Samson, D. Burke, P. Tourney, N. Thaulow, S. Sahu, Predicting the microstructural degradation of concrete in marine environment, ACI Special Publication, SP-212-69 (2003) 1127-1153.

[9] A. Chabrelie, E. Gallucci, K. Scrivener, U. Müller, Durability of field concretes made of Portland and silica fume cements under seawater exposure for 25 years, in: D.H. Bager (Ed.) Nordic Exposure Sites – Input to revision of EN206-1, Workshop Proceeding from a Nordic Miniseminar, Hirtshals – Denmark, 2008.

[10] U.H. Jakobsen, Microstructural surface deterioration of concrete exposed to seawater: results after 2 years exposure, in: U.H. Jakobsen (Ed.) Proceedings of the 14th Euroseminar on Microscopy Applied to Building Materials, , Helsingør, Denmark, 2013, pp. 62-66.

[11] K. De Weerdt, H. Justnes, M.R. Geiker, Changes in the phase assemblage of concrete exposed to seawater, Cement Concrete Compos, 47 (2014) 53-63.
[12] J. Stark, B. Möser, F. Bellmann, C. Rössler, Thermodynamische Modellierung der Hydratation von OPC, in: Q.C.d. Zementhydratation (Ed.) 16 Internationale Baustofftagung (ibausil), Weimar, Germany, 2006, pp. 1-0047-0041-0066.
[13] P.W. Brown, The system Na_2O-CaO-SiO_2-H_2O, J Am Ceram Soc, 73 (1990) 3457-3461.
[14] G. Plusquellec, M.R. Geiker, J. Lindgård, J. Duchesne, B. Fournier, K. De Weerdt, Determination of the pH and the free alkali metal content in the pore solution of concrete: Review and experimental comparison, Cement Concrete Res, 96 (2017) 13-26.
[15] D. Kulik, T. Wagner, S. Dmytrieva, G. Kosakowski, F. Hingerl, K. Chudnenko, U. Berner, GEM-Selektor geochemical modeling package: revised algorithm and GEMS3K numerical kernel for coupled simulation codes, Computational Geosciences, 17 (2013) 1-24.
[16] T. Wagner, D.A. Kulik, F.F. Hingerl, S.V. Dmytrieva, GEM-Selektor geochemical modeling package: TSolMod library and data interface for multicomponent phase models, Canadian Mineralogist, 50 (2012) 1173-1195.
[17] T. Thoenen, W. Hummel, U. Berner, E. Curti, The PSI/Nagra Chemical Thermodynamic Data Base 12/07, PSI report 14-04, Villigen PSI, Switzerland, 2014.
[18] T. Thoenen, D.A. Kulik, Nagra/PSI Chemical Thermodynamic Data Base 01/01 for the GEM-Selektor (V.2- PSI) Geochemical Modeling Code: Release 28-02-03. Internal Report TM-44-03-04, available from: http://gemswebpsich/GEMS3/doc/pdf, (2003).
[19] B. Lothenbach, D. Kulik, T. Matschei, M. Balonis, L.G. Baquerizo, B.Z. Dilnesa, G.D. Miron, D. Myers, Cemdata18: A thermodynamic database for hydrated Portland cements and alkali-activated materials, Cem Concr Res, (2018) submitted.
[20] D.A. Kulik, Improving the structural consistency of C-S-H solid solution thermodynamic models, Cem Concr Res, 41 (2011) 477-495.
[21] D. Nied, K. Enemark-Rasmussen, E. L'Hôpital, J. Skibsted, B. Lothenbach, Properties of magnesium silicate hydrates (M-S-H), Cem Concr Res, 79 (2016) 323-332.
[22] B. Lothenbach, E. Bernard, U. Mäder, Zeolite formation in the presence of cement hydrates and albite, Phys Chem Earth, 99 (2017) 77-94.
[23] W. Kunther, B. Lothenbach, K. Scrivener, On the relevance of volume increase for the length changes of mortar bars in sulfate solutions, Cem Concr Res, 46 (2013) 23-29.
[24] Z. Shi, M.R. Geiker, B. Lothenbach, K. De Weerdt, S. Ferreiro, K. Enemark-Rasmussen, J. Skibsted, Friedel's salt profiles from thermogravimetric analysis and thermodynamic modelling of Portland cement-based mortars exposed to sodium chloride solution, Cem Conc Comp, 78 (2017) 73-83.

[25] U.H. Jakobsen, Phase assemblage analysis of concrete submerged in seawater for 5 years, in: 6th EMABM Euroseminar on Microscopy Applied to Building Materials, Les Diablerets, 2017, pp. 76-80.
[26] N.R. Buenfeld, J.B. Newman, The development and stability of surface layers on concrete exposed to sea-water, Cement Concrete Res, 16 (1986) 721-732.
[27] E. L'Hôpital, B. Lothenbach, K. Scrivener, D.A. Kulik, Alkali uptake in calcium alumina silicate hydrate (C-A-S-H), Cement Concrete Res, 85 (2016) 122-136.
[28] U.H. Jakobsen, K. De Weerdt, M.R. Geiker, Elemental zonation in marine concrete, Cement Concrete Res, 85 (2016) 12-27.
[29] K. Byfors, Chloride binding in cement paste, Nordic Concrete Res, 5 (1986) 27-38.
[30] H. Zibara, Binding of external chlorides by cement paste, Thesis Department of Civil Engineering, University of Toronto, National Library of Canada, 2001.
[31] K. De Weerdt, D. Orsáková, M.R. Geiker, The impact of sulphate and magnesium on chloride binding in Portland cement paste, Cement Concrete Res, 65 (2014) 30-40.
[32] K. De Weerdt, A. Colombo, L. Coppola, H. Justnes, M.R. Geiker, Impact of the associate cation on chloride binding of Portland cement paste, Cement Concrete Res, 68 (2015) 196-202.
[33] Z. Shi, M.R. Geiker, K. De Weerdt, T. Østnor, B. Lothenbach, F. Winnefeld, J. Skibsted, Role of calcium on chloride binding of hydrated Portland cement – metakaolin limestone blends, Cem Concr Res, 95 (2017) 205-216.
[34] F.J. Millero, R. Feistel, D.G. Wright, T.J. McDougall, The composition of Standard Seawater and the definition of the Reference-Composition Salinity Scale, Deep Sea Research Part I: Oceanographic Research Papers, 55 (2008) 50-72.

535 **Tables**

536

537 **Table 1: Mix composition of the tested mortars including the water-to-binder mass ratio (w/b).**

	Mass [g]
PC	1522.8
SF	97.2
water	638.6
sand	4050.0
SP	4.9
demper	6.1
w/b	0.40

538

539

Table 2: Chemical composition [wt.%] and physical characteristics of the Portland cement (PC), fly ash (FA), slag, silica fume (SF) and sand.

[%]	PC	SF	sand
LOI 950C	2.4	2.0	0.3
SiO_2	19.6	95.1	95.8
Al_2O_3	4.5	1.0	1.6
TiO_2	0.3	0.0	0.1
MnO	0.1	0.0	0.0
Fe_2O_3	3.5	0.1	0.7
CaO	61.6	0.1	0.1
MgO	2.4	0.4	0.1
K_2O	1.0	1.0	0.7
Na_2O	0.5	0.1	0.0
SO_3	3.4	0.0	0.0
P_2O_5	0.2	0.1	0.0
CO_2	1.0		
free CaO	2.5		
K_2O water soluble	0.9		
Na_2O water soluble	0.3		
Blaine [cm^2/g]	3900		
density [g/cm^3]	3.12	2.3	2.66
BET [m^2/g]		19.19	

Table 3: The mineral composition of the ordinary Portland cement (PC) determined by XRD-Rietveld.

minerals	[%]
C_3S	55.7
C_2S	15.4
C_3A	5.7
C_4AF	10.9

547

548 **Table 4: Elemental composition of the exposure solutions ([1] Standard seawater composition from**
549 **Millero et al. [34] with a pH of 8.1 at 25°C, [2]by titration)**

	Seawater[1]		NaCl-solution[2]	
	[g/l]	[mmol/l]	[g/l]	[mmol/l]
C	0.025	2.1		
Ca	0.44	10.9		
Cl	20.6	580	19.3	545
K	0.42	10.8		
Mg	1.36	56.3		
Na	11.4	497	12.52	545
S	0.96	30.0		

550

551

552 **Table 5: Elemental composition of the pore solution of the mortars after 3 years of sealed curing**
553 **determined by ICP-MS on expressed pore solution.**

	Concentration [mmol/l]
Al	0.04
Ca	4.12
Cl	2.11
K	187
Mg	0.005
Na	159
Si	0.19
S	8.22
Fe	0.006

554

555

556 **Figures**

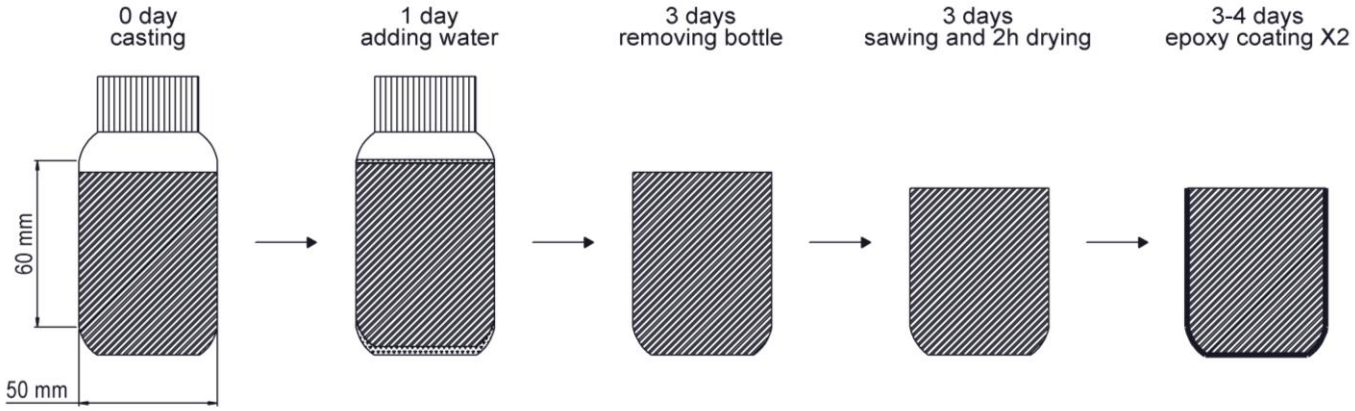

557

558 **Figure 1: Sample preparation**

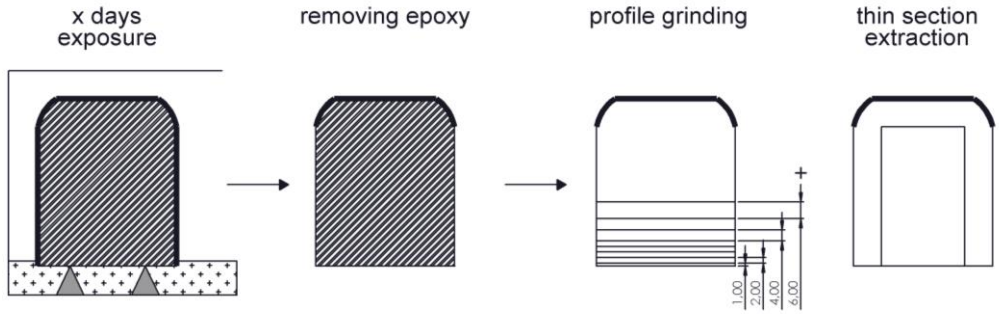

559

560 **Figure 2: Exposure conditions and sample extraction**

561

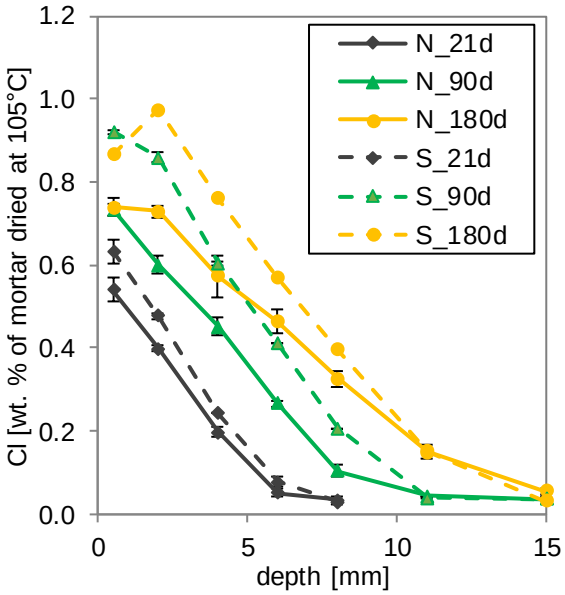

Figure 3: Total chloride profiles of PC mortar samples exposed to seawater (S) or NaCl solution (N) for 21, 90 and 180 days, expressed at wt.% of mortar dried at 105 °C.

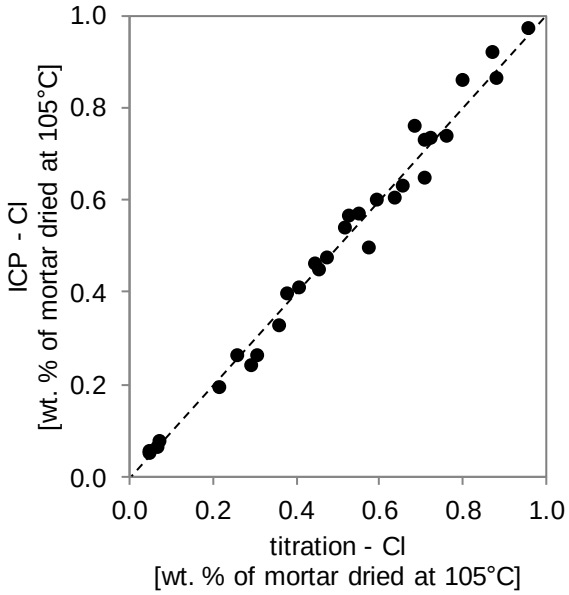

Figure 4: Comparison of the total chloride content determined by ICP-MS with the amount determined by titration on the same profile ground mortar samples.

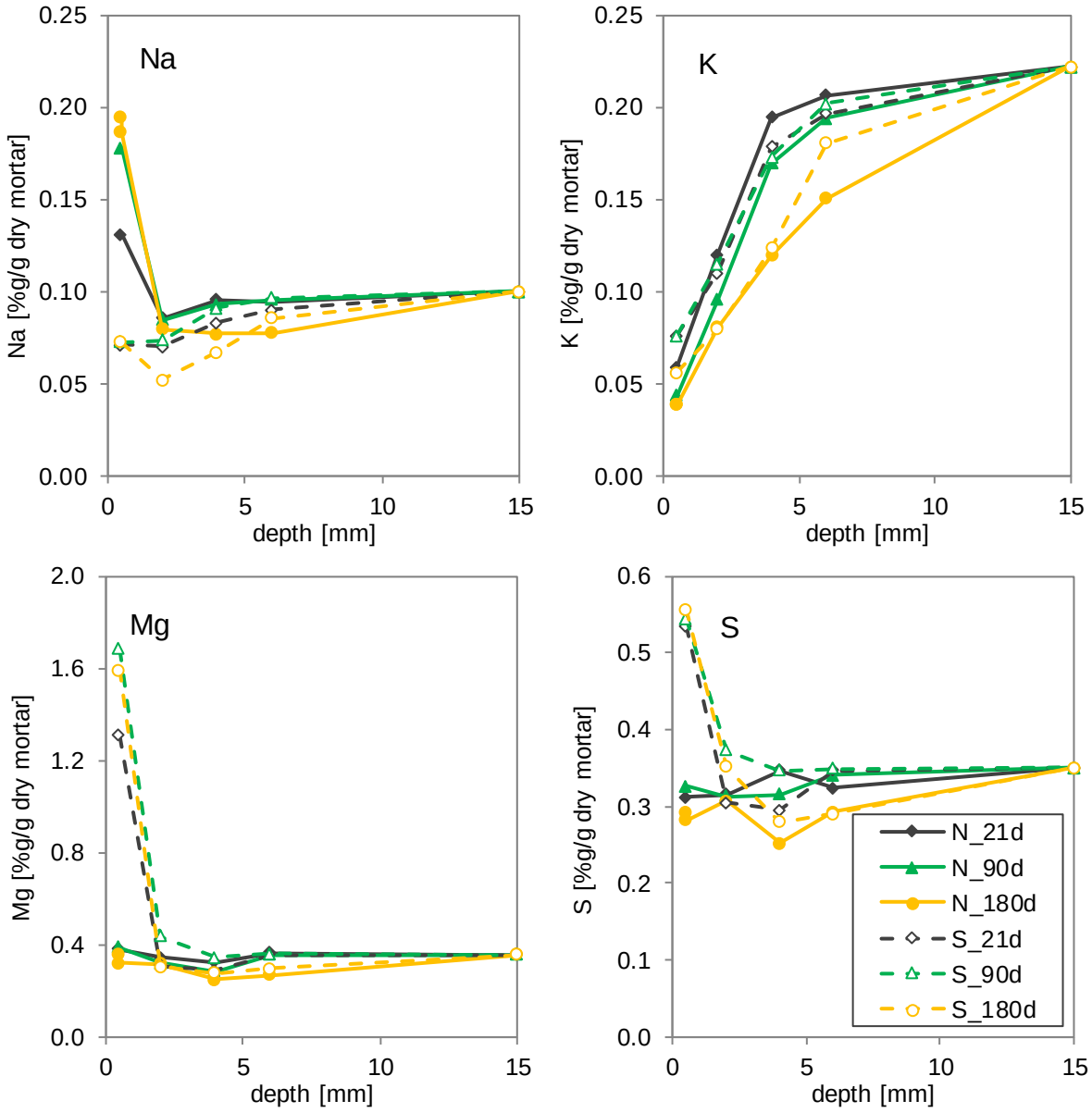

572

573

574 **Figure 5: Total sodium (Na), potassium (K), magnesium (Mg) and sulphur (S) content determined by**

575 **ICP-MS for profile ground PC mortar samples after 21, 90 and 180 days of exposure to seawater (S)**

576 **and NaCl solution (N), expressed at wt. % of mortar dried at 105 °C.**

577

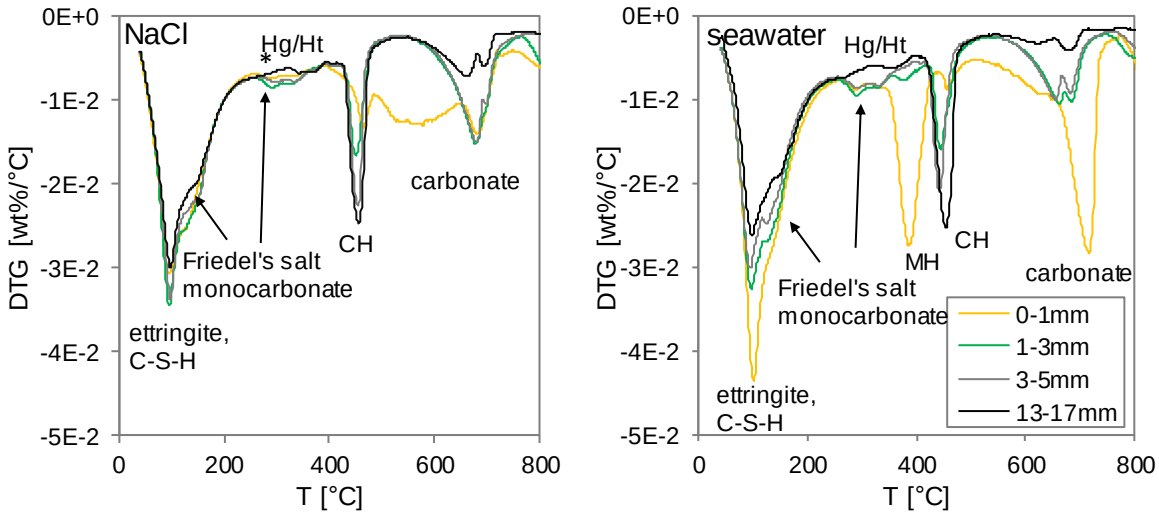

578

579 **Figure 6: Derivative of thermogravimetric curves (DTG) for different profile ground sections of the**
580 **PC mortar exposed for 90 days to NaCl solution and seawater, expressed as wt. % of the initial**
581 **mortar mass at 40 °C per °C. The weight loss peaks typically associate with the following phases as**
582 **indicated: ettringite, C-S-H, Friedel's salt, monocarbonate, portlandite (CH), brucite (MH), and**
583 **potentially M-S-H and natrolite (*). The weight loss above 550 °C is associated with the**
584 **decomposition of carbonates.**

585

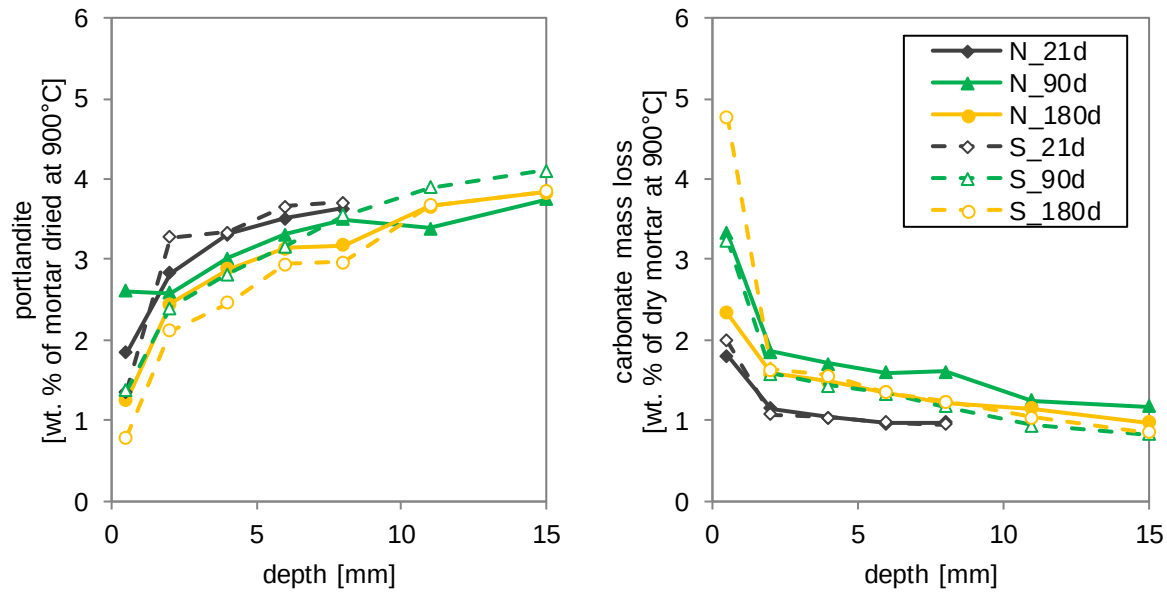

586

587 **Figure 7: Portlandite (left) and carbonate content (right) determined by TGA on profile ground PC**
588 **mortar after 21, 90 and 180 days of exposure to seawater (S) and NaCl solution (N), expressed as**
589 **wt. % of mortar dried at 900 °C.**

590

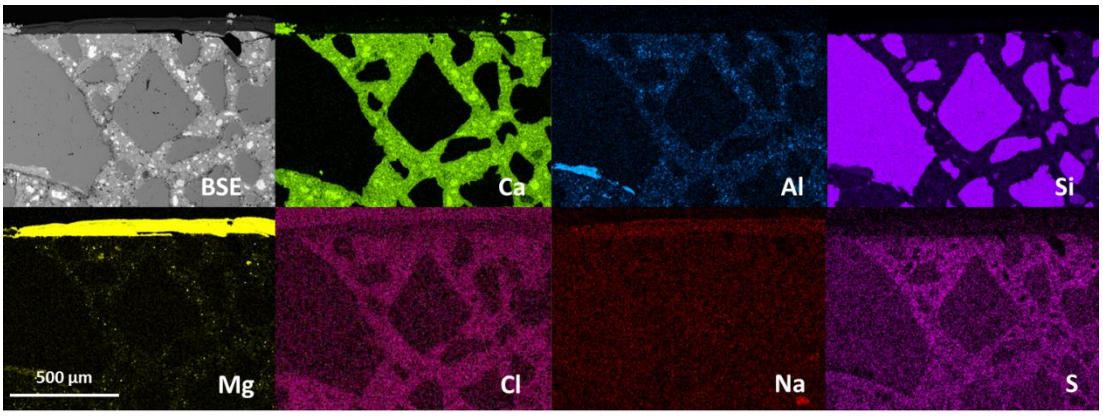

Figure 8: Elemental maps of the exposed surface of the PC mortar after 90 days of exposure to seawater. The exposed surface is at the top of the images.

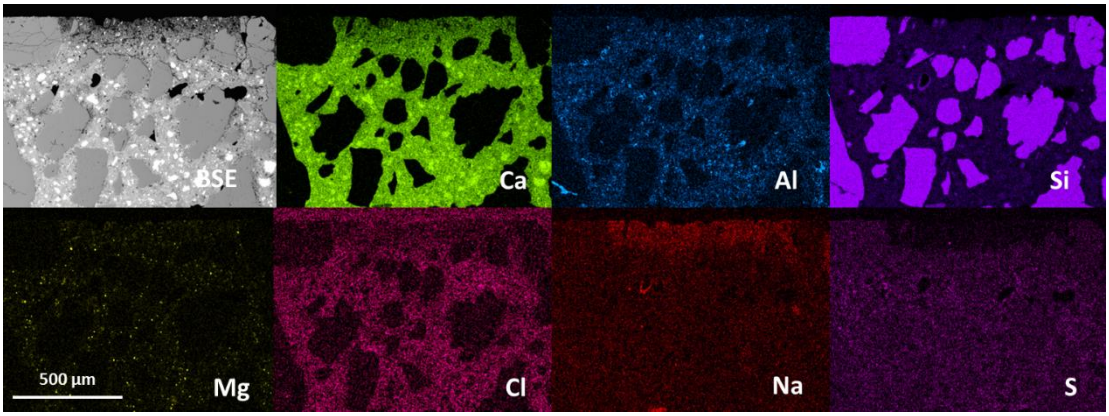

Figure 9: Elemental maps of the exposed surface of the PC mortar after 90 days of exposure to NaCl solution. The exposed surface is at the top of the images.

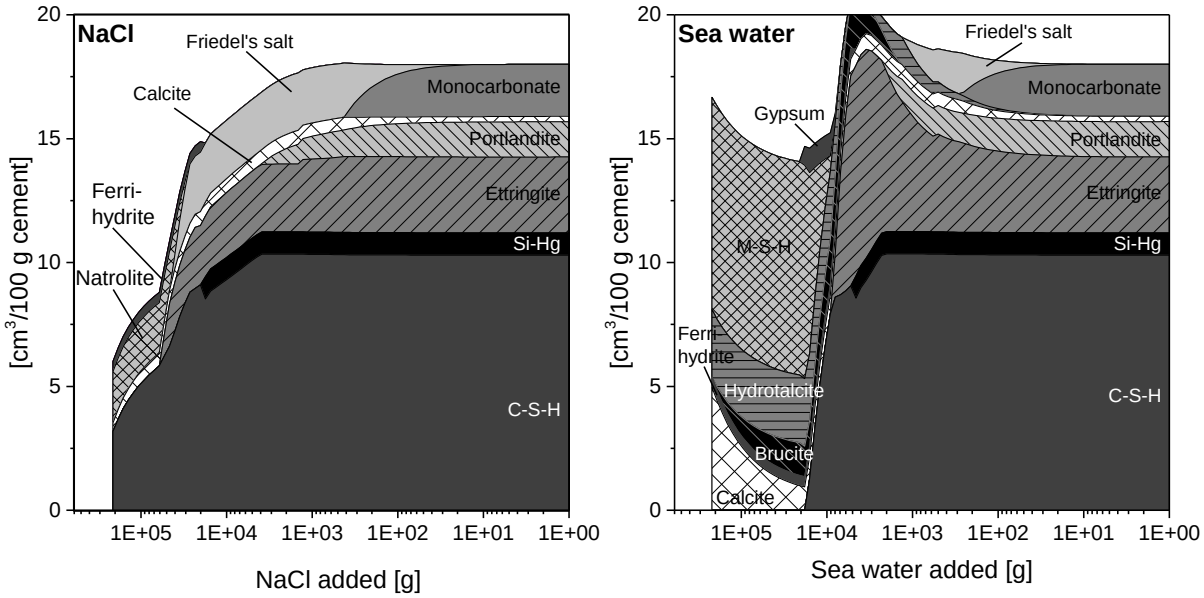

Figure 10: Predicted volume of the phases in the PC paste upon exposure to increasing amounts of NaCl solution (left) or seawater (right) in [cm³/100 g cement].

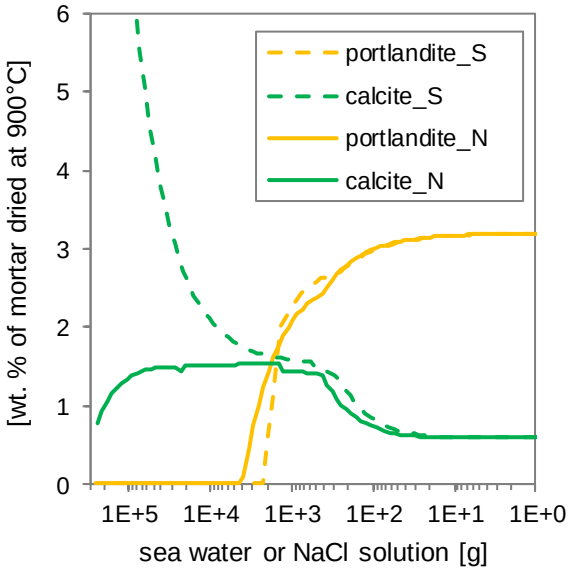

Figure 11: Predicted portlandite and calcite profiles in the PC mortar given as wt. % of mortar (including the amount of modelled bound water) upon exposure to increasing amounts of NaCl solution (_N, solid line) or seawater (_S, dotted line).

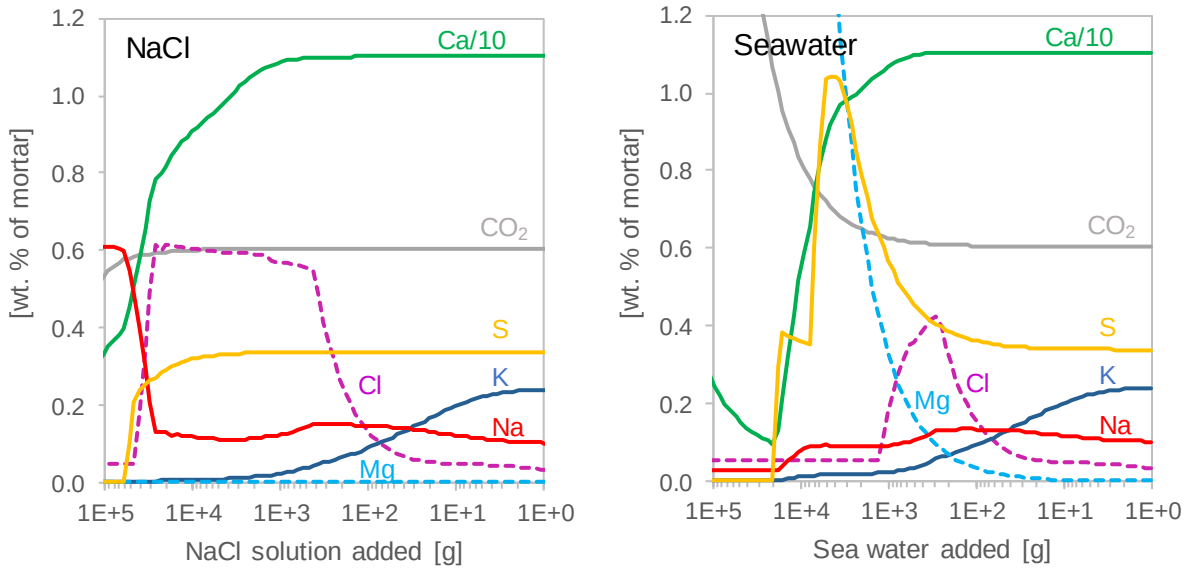

608

609 **Figure 12: Predicted elemental profiles in the cement paste given as wt. % of mortar (including the**
610 **modelled bound water and an additional 10 ml exposure solution per 100 g of cement) upon**
611 **exposure to increasing amounts of NaCl solution (left) and seawater (right).**